Clinical Cancer Research

In Vivo Detection of HSP90 Identifies Breast Cancers with Aggressive Behavior

Takuya Osada[1], Kensuke Kaneko[1], William R. Gwin[2], Michael A. Morse[3], Amy Hobeika[1], Brian W. Pogue[4], Zachary C. Hartman[1], Philip F. Hughes[5], Timothy Haystead[5], and H. Kim Lyerly[1]

Abstract

Purpose: Hsp90, a chaperone to numerous molecular pathways in malignant cells, is elevated in aggressive breast cancers. We hypothesized that identifying breast cells with elevated Hsp90 activity in situ could result in early detection of aggressive breast cancers.

Experimental Design: We exploited the uptake of an Hsp90 inhibitor by malignant cells to create an imaging probe (HS131) of Hsp90 activity by linking it to a near-infrared (nIR) dye. HS131 uptake into cells correlated with cell membrane expression of Hsp90 and was used to image molecular subtypes of murine and human breast cancers *in vitro* and in murine models.

Results: HS131 imaging was both sensitive and specific in detecting the murine 4T1 breast cancer cell line, as well as subclones with differing metastatic potential. Highly metastatic subclones (4T07) had high HS131 uptake, but subclones with lower metastatic potential (67NR, 168FARN) had low HS131 uptake. We generated isogenic cell lines to demonstrate that overexpression of a variety of specific oncogenes resulted in high HS131 uptake and retention. Finally, we demonstrated that HS131 could be used to detect spontaneous tumors in MMTV-neu mice, as well as primary and metastatic human breast cancer xenografts. HS131 could image invasive lobular breast cancer, a histologic subtype of breast cancer which is often undetectable by mammography.

Conclusions: An HSP90-targeting nIR probe is sensitive and specific in imaging all molecular subtypes of murine and human breast cancer, with higher uptake in aggressive and highly metastatic clones. Clinical studies with Hsp90-targeting nIR probes will be initiated shortly. *Clin Cancer Res; 23(24); 7531–42. ©2017 AACR.*

Introduction

Although screening mammographic techniques have undergone refinement and improvement, the conceptual framework for screening relies on detecting anatomic changes and/or tissue microcalcifications in regions of the breast. In contrast, molecular changes associated with malignant behavior, termed the "Hallmarks of Cancer" (1), occur prior to detectable anatomic change (2), but the practical detection of these molecular signals *in vivo* has been limited.

Rather than detecting anatomic abnormalities, we proposed to detect the presence of a chaperone of multiple oncogenic signaling molecules, specifically detecting Hsp90 as a diagnostic molecular marker to distinguish malignant breast cells from normal tissues. Hsp90 is attractive as it has a role in chaperoning over 400 putative client proteins, many of which regulate signaling pathways governing cellular growth and differentiation (3–7).

It has been previously demonstrated that high HSP90 expression in primary breast cancer identifies a population of patients with decreased survival (8). In addition, our own group has reported that upregulation of HSP90 expression independently associated with an increased risk of recurrence of TNBC and was associated with poor prognosis in patients with $HER2^{-}/ER^{+}$ breast cancer (9). The role of Hsp90 in mediating malignant behavior may be the result of oncogene-driven factors that alter its normal cellular behavior (10). Hyperactivation is postulated to result in an increased affinity for ATP and Hsp90 inhibitors and the expression of ectopic Hsp90 (11, 12). If oncogenically activated Hsp90 precedes malignant behavior in vivo, this could be used diagnostically as one of the earliest indicators of truly malignant cells (13–15).

To image Hsp90, we chose an analogue of the small-molecule inhibitor, SNX-5422, already known to bind with high affinity to the ATP-binding domain of Hsp90 to which we linked a near-infrared (nIR) probe (HS131; ref. 16). An advantage of this strategy is that a small-molecule probe would not be limited by perfusion, as the distribution of a small molecule may be by diffusion. We tested its ability to image murine and human breast cancers *in vitro* and *in vivo* (17–20).

Materials and Methods

Reagents

Hsp90 inhibitors tethered to fluorophores or radioiodine to detect Hsp90 *in vivo* have been developed (21). For the potential

[1]Department of Surgery, Duke University Medical Center, Durham, North Carolina. [2]Tumor Vaccine Group, Center for Translational Medicine in Women's Health, University of Washington, Seattle, Washington. [3]Department of Medicine, Duke University Medical Center, Durham, North Carolina. [4]Thayer School of Engineering, Dartmouth College, Hanover, New Hampshire. [5]Department of Pharmacology and Cancer Biology, Duke University, North Carolina.

Note: Supplementary data for this article are available at Clinical Cancer Research Online (http://clincancerres.aacrjournals.org/).

Corresponding Author: H. Kim Lyerly, Duke University Medical Center, 203 Research Drive, Rm 433B Box 2606, Durham, NC 27710. Phone: 919-681-8350; Fax: 919-681-7970; E-mail: kim.lyerly@duke.edu

doi: 10.1158/1078-0432.CCR-17-1453

Translational Relevance

Breast cancer screening is performed by mammographic imaging which detects anatomic changes; however, molecular alterations associated with aggressive behavior precede these anatomic abnormalities. The modalities to detect these molecular alterations, many of which are associated with oncogenic signaling, are unavailable clinically. An imaging strategy that could detect a chaperone linked to a broad range of signaling molecules, such as Hsp90, could be a promising approach to detect early aggressive breast cancers. We demonstrate that a novel near-infrared dye tethered Hsp90 inhibitor (HS131) is able to detect oncogene-driven breast cancers, including multiple different molecular subtypes of human breast cancers. Stronger uptake was observed in cancers with higher metastatic potential. Importantly, HS131 could image spontaneously arising breast cancer in murine models. Our data support a clinical trial of Hsp90-targeted imaging to detect aggressive, early breast cancer.

clinical application as an *in vivo* imaging reagent, we developed a new compound with a nIR dye tethered to an Hsp90 ligand, denoted HS131. It has an excitation wavelength of 640 nm and an emission wavelength of 680 nm that would allow tissue penetration, and visualization of breast lesions in preclinical models. To control for nonspecific dye uptake, HS152, a nIR dye lacking an Hsp90 binding moiety, was used as a control. An FITC-tethered Hsp90 inhibitor (HS27) was previously developed (21) and used in cell labeling *in vitro* for comparison with HS131. The synthesis of HS131 and HS152 are described previously (16).

Breast cancer cell lines and culture

Human breast cancer cell lines with different molecular subtypes, luminal (MCF-7, T-47D), $HER2^+$ (BT474M1, KPL-4), and triple negative (MDA-MB-231, MDA-MB-468), were used in imaging experiments of human breast cancer xenografts. MCF-7, T-47D, MDA-MB-231, and MDA-MB-468 were purchased from the ATCC and were cultured as recommended by ATCC. BT474M1 cell line was a more tumorigenic and metastatic subclone of BT474, and a kind gift from Dr. Dihua Yu in University of Texas MD Anderson Cancer Center (Houston, TX; ref. 22). KPL-4 cell line was a kind gift from Dr. Junichi Kurebayashi (Kawasaki Medical School, Japan; ref. 23).

The murine breast cancer cell line, 4T1 (CRL-2539), was purchased from ATCC. Sublines 4T07, 67NR, and 168FARN, were obtained from the laboratory of Dr. Gregory Hannon (Howard Hughes Medical Institute, Cambridge, MA). Tumor subpopulation lines 67, 168, 66, and 410.4 were isolated from a single, spontaneously arising mammary tumor in a BALB/cfC3H mouse (24). Sublines 4T1 and 4T07 (both thioguanine-resistant) were derived from the parental population 410.4, and sublines 168FARN (diaminopurine-resistant) was selected from the parental populations 168. The geneticin-resistant subline 67NR was obtained by transfection of line 67. These subpopulations are phenotypically heterogeneous in their metastatic behavior but share a common origin (24). 4T1 cell line is highly metastatic to lung, liver, bone, and brain, whereas 4T07 cells metastasize to lymph nodes, liver and spleen 8 weeks after orthotopic implantation to the mammary fatpad (Supplementary Table S1). 168FARN is only weakly metastatic and 67NR is a nonmetastatic subline. 4T1 and other sublines were maintained in culture in DMEM supplemented with 10% FBS and 1% penicillin/streptomycin.

MM3MG cell line (CRL-6376), purchased from ATCC, was used as a representative premalignant murine mammary epithelial cell to assess the effects of potential oncogenic genes. Retroviral vectors encoding several known oncogenes (HER2, HRAS-V12, Myc-T58A, EGFR-L858R, and Luciferase) were obtained from Addgene or constructed by ourselves (details available upon request) and prepared using standard transient transfection and purification procedures. MM3MG cells were transfected using concentrated retroviral vectors and polybrene (10 μg/mL working concentration) overnight using standard procedures, followed by selection of cells using puromycin (2 μg/mL) or by flow cytometry–based sorting for HER2-infected cells. Cells were maintained in culture in DMEM supplemented with 10% FBS, 1% penicillin/streptomycin, and 2 μg/mL of puromycin.

All cell lines listed above were routinely inspected for phenotypic variation and mycoplasma contamination.

Patient-derived breast cancer xenografts, HCI-013 EI and HCI-019, were purchased from Oklahoma Medical Research Foundation (Oklahoma City, OK) and maintained in SCID mice.

Animals

SCID-beige mice were originally purchased from Charles River. BALB/c mice and MMTV-neu mice were purchased from Jackson Laboratory, and maintained in the Duke University Cancer Center Isolation Facility in accordance with the Institutional Animal Care and Use Committee guidelines. All experiments were conducted and mice were euthanized according to IACUC-approved protocols.

For the imaging study of murine breast cancer cells, including 4T1, 4T07, 67NR, and 168FARN, female BALB/c mice were subcutaneously injected with cells ($0.3–10 \times 10^6$ cells/injection). For the imaging of spontaneous breast cancers, MMTV-neu female mice were maintained in our animal colony for over 10 months, and tumor growth was monitored. Once the tumor sizes reached 10 mm in diameter, mice were used for imaging.

For the imaging of human breast cancer xenografts, including MCF-7, T-47D, BT474M1, KPL-4, MDA-MB-231, and MDA-MB-468, $1–3 \times 10^6$ cells were resuspended in 50% Matrigel/50% saline, and subcutaneously injected to the flank of SCID-beige mice. For MCF-7, T-47D, BT474M1, and KPL-4 cells, to assist the growth of tumors, 0.72-mg estrogen pellet (17β-estradiol, 90 day-release; Innovative Research America) was implanted to the back of each mouse using trocar.

Fluorescence imaging and measurement

For the imaging of tumors in mice, HS131 or HS152 (10–25 nmol) were dissolved in DMSO (20 μL per injection) and administered to mice via tail vein. Mouse whole-body images were taken over time using IVIS Lumina imaging system (PerkinElmer) while mice were anesthetized with the combination of ketamine/xylazine or with 2% isoflurane. For HS131 and HS152, 640-nm excitation filter and Cy5.5 emission filter was used, and exposure time varied from 0.1 to 1 second depend on the fluorescence intensity. For some experiments, *ex vivo* imaging was performed with excised tumors and organs put into the plate. Fluorescence signals were analyzed

using Living Image 4.0 (PerkinElmer) by quantifying the average radiant efficiency ([p/s/cms/sr]/[μW/cms]) at the selected region of interest covering the tumor area or organs.

The LI-COR Pearl Trilogy Imager (LI-COR Biosciences) was also used for the detection of fluorescence signals from the tumor-bearing mice injected with HS131 or HS152. Mice were anesthetized with 2% isoflurane, and whole-body image was taken using 700-nm channel. Fluorescence signals were analyzed using ImageStudio software (version 5.0.21). The selected regions of interest covering the tumor area or organs were analyzed for the fluorescence intensity and fluorescence intensity per area.

Flow cytometry

Tumor cells cultured *in vitro* were harvested with 0.05% trypsin/EDTA, and washed with PBS three times. Cells were resuspended in the medium, and HS131 or HS152 were added to the medium to make the final concentration of 10 μmol/L. Cells were incubated in a CO_2 incubator at 37°C for 30 minutes, washed with PBS three times, and soon acquired by LSRII flow cytometry machine (red laser, APC channel, filter 660/20; BD Biosciences). Data analysis was performed using the FlowJo software. For the analysis of Hsp90 expression on the cell surface, cells were incubated with phycoerythrin (PE)-conjugated anti-Hsp90 mAb (clone AC88, Abcam) for 30 minutes at 4°C. PE-conjugated IgG isotype control was used as a negative control staining.

For the analysis of tumor cells from *in vivo* tumors, tumors were minced with razor blade and digested for 1.5 hours at 37°C with triple enzyme buffer, which includes collagenase III (1 mg/mL, Worthington), hyaluronidase (0.1 mg/mL, Sigma), and deoxyribonuclease (20 U/mL, Sigma). Tumor digests were passed through 40-μm cell strainer, washed with PBS three times, and acquired by LSRII flow cytometry machine (BD Biosciences).

Fluorescence microscopy analysis

Formalin-fixed tumor tissues were cut into sections with 30-μm thickness using Vibratome, and observed under Zeiss LSM780 confocal laser microscope with HeNe 633 nm laserPerki. Frozen sections of tumor tissues with 5-μm thickness were also used for histologic analysis. Sections were briefly fixed with 10% formalin, and DAPI-containing mounting buffer (Vector Laboratories) was applied. Tissue sections were analyzed using Zeiss Axio Observer Microscope with Cy5 cube (excitation: BP640/30, beam splitter: FT660, emission: BP690/50).

Statistical analysis

The differences in the fluorescence intensities in imaging studies were analyzed using the Student *t* test.

Results

Biodistribution of HS131 to normal tissue and breast tumors in mice

We constructed a novel nIR-tethered Hsp90 inhibitor (subsequently referred to as HS131; Fig. 1A). As a control compound, we generated HS152, which consists of the same nIR dye and a linker but no Hsp90 inhibitor.

To determine the normal tissue distribution of HS131, we injected HS131 or control HS152 (10 nmol per injection) into nontumor-bearing mice via the tail vein. Twenty-four hours after intravenous injection, mice were euthanized and organs/tissues were collected. Mice not injected with HS131 or HS152 were used as another control to determine the background level of nIR signals. Tissues/organs, including eyes, brain, heart, lung, liver, spleen, kidney, gut, urinary bladder and skin, were imaged *ex vivo* by the IVIS imager machine, an imaging modality that detects IR at 640 nm. Two representative cases for each treatment group (HS131 vs. HS152 vs. no injection) are shown in Fig. 1B. To compare the tumor uptake of HS131 and HS152, 4T1 tumor-bearing mice were administered with these Hsp90 probes (10 nmol/injection), and images were taken at 6-hour time point (Fig. 1C, left). Strong accumulation of HS131 was confirmed in the 4T1 tumors, while HS152 did not show detectable accumulation. We also detected nIR signals from the liver and upper intestine, where HS131-containing bile accumulated. At 24 hours after Hsp90 probe injection, mice were euthanized and nIR signals in 4T1 tumors were analyzed *ex vivo* (Fig. 1C, right). Again, HS131 accumulation in the tumors was confirmed, while nIR signals from tumors of HS152-injected mice had similar levels to those of the noninjected control. Compared with the nIR signal levels observed in 4T1 breast tumors in the same imaging condition (above 2.3×10^8 average radiant efficiency; Fig. 1D, right), the nIR signals detected in these organs were very weak (maximum 1.2×10^8 average radiant efficiency). Among these organs, HS131 injection induced slightly stronger nIR signals in lung and liver compared with HS152 or the noninjected control (Fig. 1D). We repeated the biodistribution testing of HS131 and HS152 in 4T1 tumor-bearing mice (Supplementary Fig. S1). We confirmed similar distribution of these probes to the organs, and 4T1 tumors showed higher nIR signals than the organs in HS131 injected mice at the 24-hour time point. We also conducted *in vivo* imaging of 4T1 tumors using HS198, an inactive analogue of HS131, which lacks the capacity to bind Hsp90 protein (16). *In vivo* tumor uptake of HS198 was similar to that of the control probe HS152 (Supplementary Fig. S2), and thus we used HS152 as a control for HS131 in the following experiments.

Hsp90-based probe binds to aggressive murine breast cancers *in vitro* and *in vivo*

We tested whether imaging by HS131 could detect aggressive murine breast cancers *in vitro* and *in vivo*. First, we tested the *in vitro* labeling of murine breast cancer line, 4T1, and its subclones with different aggressiveness (4T07, 67NR, 168FARN). Tumor cells were incubated with HS131 or HS152 at 10 μmol/L concentration in the medium, then washed intensively with PBS, and evaluated by flow cytometry. 4T1 and 4T07, the subclones with higher metastatic potential, stained more strongly with HS131, compared with the less metastatic/slower growing subclones 67NR and 168FARN (Fig. 2A). A similar relationship was observed for *in vitro* labeling by HS27 (FITC-tethered Hsp90 probe; ref. 21), and the cell surface expression of Hsp90.

To study the uptake of HS131 *in vivo* by the murine breast cancer subclones with different metastatic capacities, HS131 (10 nmol/injection) was intravenously administered 24 hours after subcutaneous implantation of tumor cells and images were taken 6 hours later (Fig. 2B). Corresponding to *in vitro* labeling with HS131, *in vivo* labeling of injected tumor cells showed stronger nIR signals in the 4T1 and 4T07 tumor cells with stronger metastatic potential, but the less aggressive subclones showed relatively weaker nIR signals. To confirm these results for tumors growing a longer period of time, and therefore with greater encapsulation and infiltration by host stroma, HS131 injection was also performed 3 days after tumor cell implantation

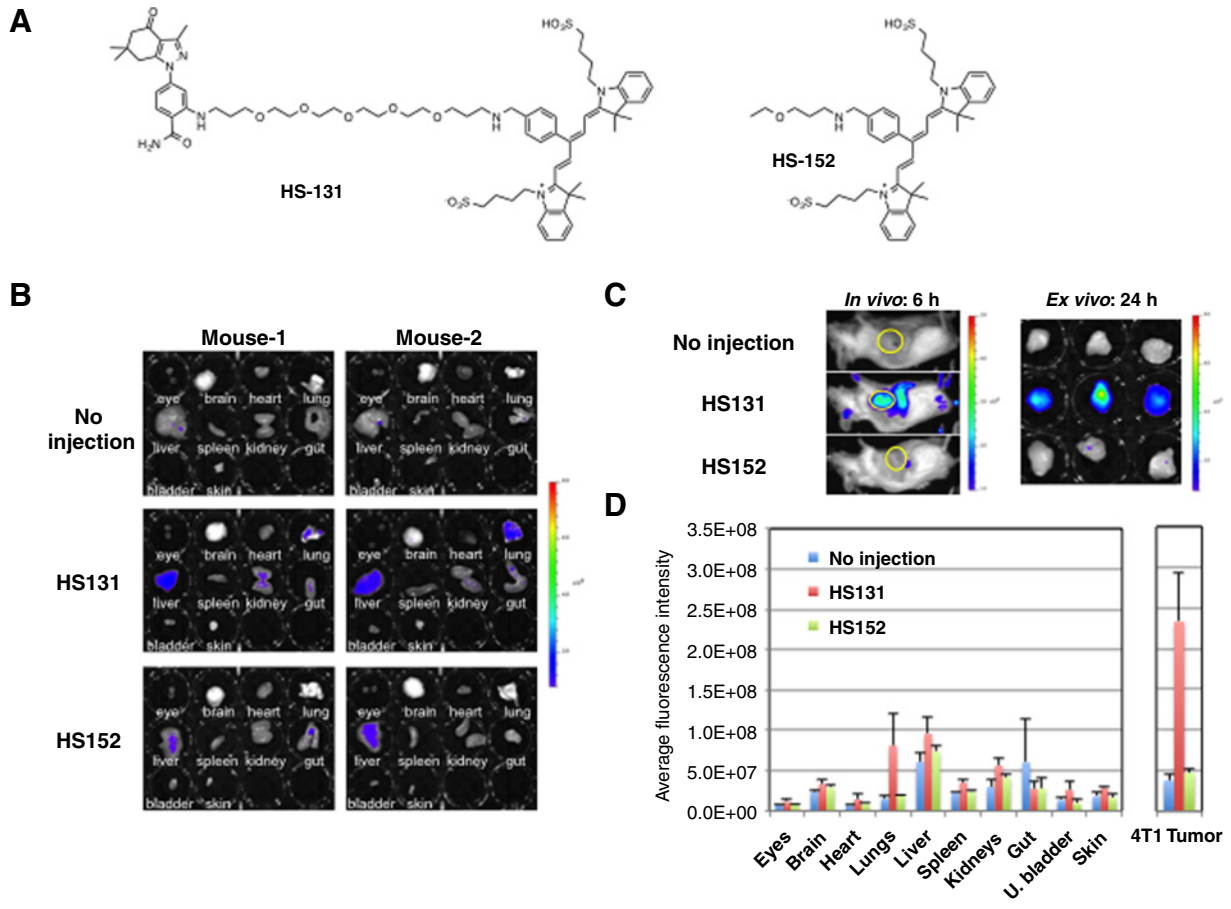

Figure 1.

Tissue distribution of HS131 and HS152 in mice. **A,** Chemical structure of HS131 and control HS152. HS131 was made by conjugating nIR dye to Hsp90 inhibitor, HS10, by peg linker. Structure of the control compound, HS152, is also shown. **B,** Tissue distribution of HS131 and control HS152 after intravenous injection in nontumor–bearing mice. HS131 or HS152 (10 nmol in 20 μL) was intravenously injected to the BALB/c mice via tail vein. Twenty-four hours later, mice were euthanized and tissues/organs (eyes, brain, heart, lung, liver, spleen, kidneys, gut, urinary bladder, skin) were harvested. nIR signal was detected *ex vivo* by IVIS machine (640 nm, Cy5.5, 1.0 sec exposure). Representative two cases for each group are shown. **C,** Tumor distribution of HS131 and control HS152 after intravenous injection in 4T1-tumor bearing mice. HS131 or HS152 (10 nmol in 20 μL) was intravenously injected into the 4T1 tumor-baring BALB/c mice via tail vein. Six hours later, nIR signals were detected by IVIS imager (640 nm, Cy5.5 filter, 1.0-second exposure). Tumor areas are marked with yellow circles. At 24-hour time point, mice were euthanized and harvested tumors were analyzed *ex vivo* by IVIS machine (640 nm, Cy5.5, 1.0-second exposure). Representative three tumors for each group were analyzed. **D,** Average florescence intensity of organs harvested from mice 24 hours after HS131 or HS152 injection. Eyes. brain, heart, lung, liver, spleen, kidney, gut, urinary bladder, and skin were collected from mice injected with HS131 or HS152 (3 mice per group). Mice without injection of Hsp90 compounds were used as negative control. For comparison, typical nIR signal levels of 4T1 tumors excised from HS131 or HS152 injected (10 nmol/mouse) tumor-bearing mice are shown in the right panel.

into the flank (images not shown). nIR signals from the tumor cell–injected areas were plotted for each cell line for day 1 and day 3 (Fig. 2C). Imaging on day 3 showed similar results with imaging on day 1. The 4T1 and 4T07 cells showed stronger labeling with HS131, while other subclones, 67NR and 168FARN, were only weakly labeled.

To confirm that nIR signals from the tumor cell injected areas on the whole-body imaging did indeed correspond with the nIR signals from tumor cells implanted into the flank, mice were euthanized after whole-body imaging and the tumor cell aggregates in the injected area of the flank were collected, and imaged *ex vivo*. As shown in Fig. 2D, nIR signals from those collected tumor cell aggregates showed similar trends with whole body imaging. 4T1 and 4T07 cells aggregates labeled stronger than other subclones. There was no clear change in nIR signal levels from day 1 to day 3 in 4T1 and 4T07 tumor cells; however, the other subclones showed moderate decreases in nIR signals (Fig. 2E).

Next, to confirm the correlation between malignant phenotype and uptake of HS131, we established murine breast epithelial cell lines transformed with various oncogenes. MM3MG cells were lentivirally transduced to express luciferase (MM3MG-Luc), Myc (MM3MG-Myc), Hras (MM3MG-Hras), EGFR (MM3MG-EGFR), and HER2 (MM3MG-HER2). *In vitro* colony formation assays showed more aggressive cell proliferation in oncogene-transduced MM3MG cells. These cells were incubated in the presence of HS131 (10 μmol/L) and nIR signals were analyzed by flow cytometry. Experiments were repeated four times, and the mean fluorescence intensity (MFI) of the HS131 signal of the oncogene-transduced MM3MG cells was compared with that of the MM3MG-Luc cells in each experiment. In Fig. 2F,

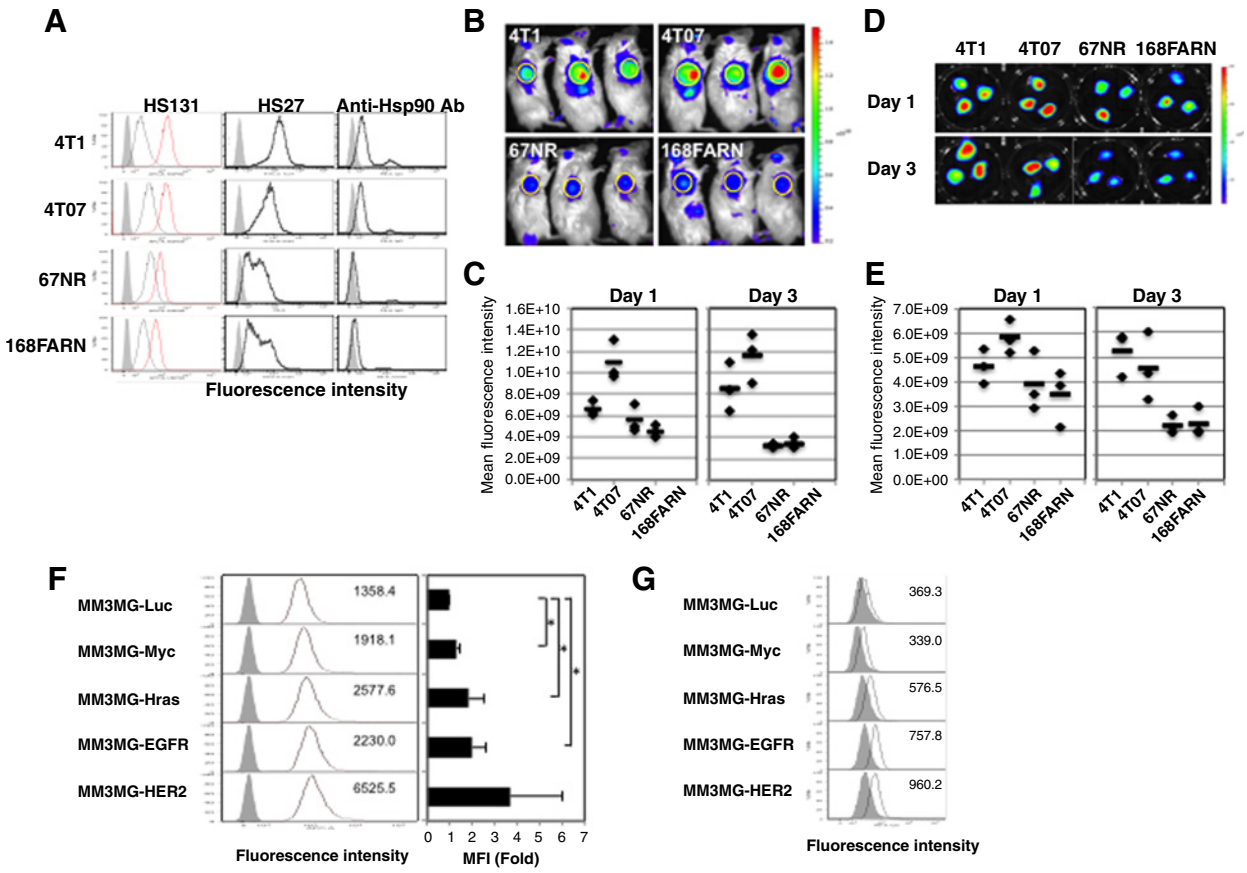

Figure 2.

In vitro labeling of murine breast cancer subclones and murine breast epithelial cells with HS131. **A,** *In vitro* labeling of 4T1 and subclone cells with HS131. 4T1 cells and subclones were harvested from the flasks and resuspended in 1% BSA/PBS buffer. HS131 or HS152 was added to the cell suspension to make 10 μmol/L final concentration. Cells were incubated at 37°C for 30 minutes and then washed with PBS three times. FITC-conjugated Hsp90 inhibitor (HS27) was used to label these cell lines for comparison purpose. Hsp90 expression on tumor cell surface was analyzed by staining cells with PE-conjugated anti-Hsp90 mAb for 30 minutes at 4°C. Cells were acquired by LSRII flow cytometry machine. Left histograms, red line: HS131, open black: HS152, gray filled: no staining. Middle histograms, open black: HS27, gray filled: no staining. Right histograms, open black: anti-Hsp90, gray filled: control IgG. **B,** *In vivo* imaging of subcutaneously implanted tumor cells with HS131 (10 M cells, 25 nmol/mouse, 6 hours). 4T1 cells and subclones (1×10^7 cells in 100-μL saline) were subcutaneously injected to the flank of BALB/c mice. On day 1 or 3, HS131 (25 nmol/20 μL) was injected via tail vein, and 6 hours later, nIR signals were detected by IVIS imager (640 nm, Cy5.5 filter, 0.2-second exposure). Tumor cell–injected areas are marked with yellow circles. **C,** nIR signals from tumor cell–injected area (days 1 and 3). On days 1 or 3, nIR signals from tumor cell–injected areas were detected and analyzed by IVIS imager (640 nm, Cy5.5 filter, 0.2-second exposure) 6 hours after HS131 administration via tail vein. Three mice for each tumor cell line were analyzed, and average radiant efficiencies were plotted. Bars show the average of 3 mice for each tumor cell lines. **D,** *Ex vivo* imaging of tumor cell aggregates (days 1 and 3, 6 hours after HS131 injection). Soon after taking images by IVIS imager (**B**), mice were euthanized and aggregates of tumor cells were taken from the flank of mice. nIR signals from excised tumor cell aggregates were detected by IVIS imager (640 nm, Cy5.5 filter, 0.5-second exposure). **E,** nIR signals from tumor cells by *ex vivo* tumor cell imaging (days 1 and 3, 6 hours after HS131 injection). nIR signals of tumor cell aggregates were detected by IVIS imager (640 nm, Cy5.5 filter, 0.2-second exposure). Three tumor cell aggregates for each tumor cell line were analyzed, and average radiant efficiencies were plotted. Bars show the average of 3 mice for each tumor cell lines. **F,** *In vitro* labeling of murine breast epithelial MM3MG cells and transformed MM3MG cells with HS131. MM3MG-Luc cells and oncogene-transformed MM3MG cells (-Myc, -Hras, -EGFR, -HER2) were incubated *in vitro* with HS131 (10 μmol/L in medium) for 30 minutes at 37°C, and acquired by LSRII flow cytometry machine (red laser, APC channel, filter 660/20). Experiments were repeated four times. Representative flow data are shown in the left with MFI in each histogram. Open histograms show nIR signals of HS131 labeled cells, and gray filled histograms show cells with no staining. Right, the average of the ratios (MFI of tranformants to MFI of MM3MG-Luc) for each transformed MM3MG cell line. Error bar, SDs. *, $P < 0.05$. **G,** Cell surface expression of Hsp90 by oncogene-transformed breast epithelial cells. MM3MG-Luc, MM3MG-Myc, MM3MG-Hras, MM3MG-EGFR, and MM3MG-HER2 cells were stained with PE-conjugated anti-Hsp90 mAb, or PE-conjugated control IgG for 30 minutes at 4°C. After wash with PBS, cells were acquired by LSRII flow cytometry machine. Open histogram: anti-Hsp90, filled histogram: IgG control. Mean fluorescence intensity for Hsp90 staining is shown in each histogram.

representative flow data are shown in the left panel with MFI in each histogram. The right panel shows the average of the ratios (MFI of tranformants to MFI of MM3MG-Luc) for each transformed MM3MG cell line. The fluorescence intensities increased in oncogene-transduced MM3MG cells compared with control MM3MG-Luc, especially MM3MG-EGFR and MM3MG-HER2, which had higher nIR signals, suggesting more intense labeling with HS131 in more malignant breast epithelial cells. Importantly, the cell surface expression of Hsp90 protein on these transformed MM3MG cells showed a correlation with the *in vitro* uptake of HS131 by these cells (Fig. 2G).

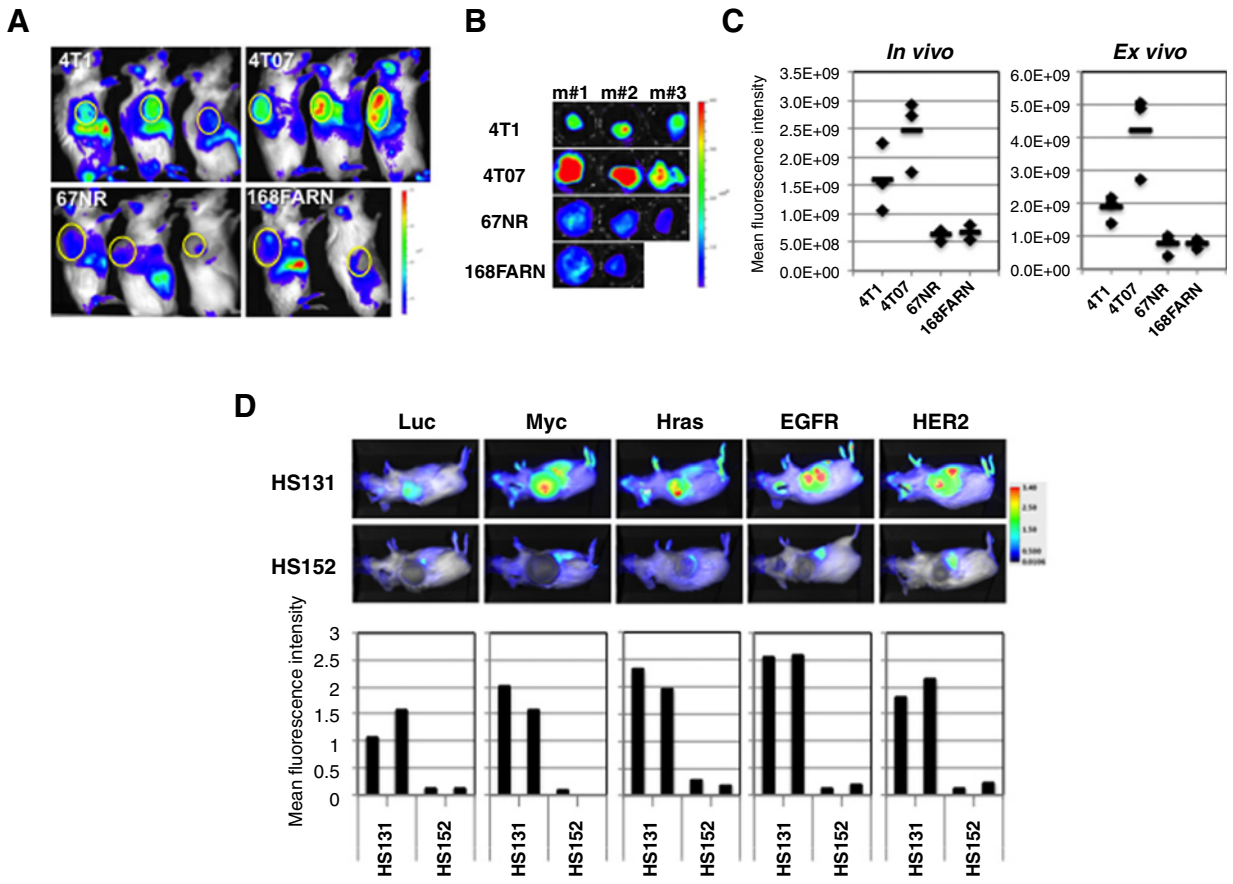

Figure 3.

In vivo labeling of murine breast cancer subclones and murine breast epithelial cells with HS131. **A,** *In vivo* imaging of subcutaneously growing breast tumors with HS131. 4T1 breast cancer cells and subclone cells (4T07, 66cl4, 67NR, 168FARN) were resuspended in saline (1×10^7 cells/100-μL saline), and injected to the flank of female BALB/c mice. Three or 2 mice were used for each cell line. After 3–5 weeks, when the tumor size reached around 10 mm in diameter, mice were injected with HS131 (10 nmol/mouse) via tail vein. Six hours later, nIR images were taken using IVIS imager machine (640 nm, Cy5.5 filter, 0.2-second exposure). Tumor areas are marked with yellow circles. **B,** *Ex vivo* imaging of 4T1 and subclone tumors with HS131. 4T1 tumor or subclone tumor-bearing mice were injected with HS131 (10 nmol/mouse) via tail vein, and 6 hours later, tumors were excised from mice after imaging with the IVIS imager. *Ex vivo* imaging of tumors were done. **C,** nIR signals from 4T1 and subclone tumors in *in vivo* and *ex vivo* imaging. (Left) nIR signal from individual tumors in *in vivo* imaging were plotted and the average values are shown as bars. (Right) nIR signal from excised tumors are plotted. Averages are shown as bars for each subclone cell line. **D,** *In vivo* nIR imaging of breast tumors of transformed MM3MG cells with HS131 and HS152. MM3MG-Luc cells and oncogene-transformed MM3MG cells (MM3MG-Myc, -Hras, -EGFR, -HER2) were implanted to the flank of SCID mice. When the tumor sizes reached around 10–12 mm in diameter, mice were injected with HS131 or HS152 (10 nmol/mouse) via tail vein. Six hours after injection, nIR signals were analyzed by LI-COR imager at 700-nm channel. Two mice for both HS131 and HS152 were tested and analyzed. MFI for each tumor is shown in the graphs.

To confirm that the imaging observations were associated with aggressiveness and not just tumor size or tumor cell number, *in vivo* imaging of established growing breast tumors were performed when the tumor diameter reached approximately 10 mm in diameter after subcutaneous injection of $1 \times 10E6$ cells into the flank. Reaching this goal diameter took 2 weeks (4T1, 4T07) to 5 weeks (168FARN). Once the tumors reached this determined size, HS131 (10 nmol) was intravenously administered to mice and whole-body imaging was performed 6 hours later. Then mice were euthanized and tumors were excised for *ex vivo* imaging. As we hypothesized, we confirmed stronger nIR signals in more aggressive 4T1 and 4T07 tumors compared with the less metastatic subclones 67NR and 168FARN of similar size (Fig. 3A–C). As surface imaging demonstrated (Fig. 3A), stronger nIR signals were confirmed in 4T1 tumors and 4T07 tumors compared with tumors of other subclones (Fig. 3B and C). Therefore, we confirmed that more aggressive tumors, such as 4T1 and 4T07, would be labeled more strongly with HS131 *in vivo* compared with less metastatic subclones, and the differences of labeling intensities are mainly derived from the biologic character of tumor cells.

To confirm that enhanced labeling of oncogene-transformed MM3MG cells by HS131 can occur *in vivo*, these transformed MM3MG cells as well as control MM3MG-Luc cells were subcutaneously implanted to the flank of female SCID-beige mice. Once the tumor sizes reached around 10–12 mm in diameter, HS131 (10 nmol/mouse) was injected via tail vein and nIR signal from each tumor was assessed (Fig. 3D). In accordance with *in vitro* cell labeling results, oncogene-transformed MM3MG tumors, especially MM3MG-EGFR tumors, demonstrated stronger nIR signals compared with MM3MG-Luc tumors, suggesting more uptake of HS131 by more aggressive tumors. Control HS152 probe did not

show a difference in the labeling of MM3MG tumors, suggesting the stronger signal in HS131-injected mice were caused by specific binding of HS131 to Hsp90 protein in tumor cells.

Hsp90-based probe HS131 binds to murine breast cancer cells *in vivo* without neovasculature

To demonstrate that detection would be diffusion limited, rather than perfusion limited, we next visualized BALB/c mice with 4T1 tumor cells implanted within 24 hours and prior to initiation of neovascularization. 4T1 cells (1×10^6 cells/10 μL saline/injection) were implanted in the mammary ducts of the second left mammary glands under stereomicroscopic direction or implanted subcutaneously in the flanks of mice. Second right mammary glands were given saline injection without tumor cells, which served as negative controls. The next day (about 18 hours later), HS131 (25 nmol/injection) was intravenously injected into mice via tail vein, and nIR images were taken 6 hours later (Supplementary Fig. S3A). Interestingly, we could detect nIR signals from the mammary glands only 1 day after intraductal implantation of 4T1 tumor cells, but not from control mammary glands (Supplementary Fig. S3A and S3C), suggesting the binding of HS131 is diffusion limited because we did not observe any neovascularization microscopically at this early time point. Similarly, subcutaneously implanted tumor cells were labeled with HS131, as shown in the right panel in Supplementary Fig. S3A. To confirm the binding of HS131 to tumors, second right and left mammary glands as well as tumor cell aggregates at the injected sites of the flank were collected after mice were euthanized, and nIR signals were analyzed *ex vivo* (Supplementary Fig. S3B and S3D). Mammary glands that received intraductal implantation of 4T1 cells showed stronger nIR signals compared with control mammary glands, confirming the binding of HS131 to tumor cells. This finding suggests the potential of HS131 to label early breast cancers even without apparent neovascularization.

Hsp90-based probe HS131 binds to spontaneously arising breast cancers in MMTV-neu mice

We also assessed the imaging efficacy of HS131 in a spontaneous murine breast cancer model. Female MMTV-neu mice at the age of approximately 8–10 months developed spontaneous breast cancer nodules, and 4 mice were chosen and HS131 or HS152 (25 nmol/injection) were administered via tail vein injection. nIR signal was analyzed through 24 hours after injection. Figure 4A shows the change of nIR signals from tumor areas, which are marked with yellow circles. nIR signal was plotted for individual tumors in Fig. 4B, demonstrating much stronger nIR signals in tumor areas in HS131 administered mice than in HS152-injected mice. Tumors were excised at 24 hours after intravenous injection of HS131 or HS152, and *ex vivo* imaging was performed (Fig. 4C). Although there was a wide variation in the nIR signal levels in spontaneous breast tumors, all tumors tended to have stronger signals with HS131 than tumors from the control HS152–injected mice. Spontaneous tumors from mice that received no compound injection showed very low nIR signals that were similar to nIR signals of tumors from HS152-injected mice (Fig. 4C). With the fluorescence microscope analysis, uptake of HS131 by tumor cells was confirmed, while tumors from HS152 injected mice showed very weak or almost no nIR signals in tumor tissues (Fig. 4D).

HS131 imaging in human breast cancer xenografts

To apply the novel imaging strategy with HS131 to the clinic, we administered HS131 to SCID-beige mice bearing human breast cancer xenografts of different molecular subtypes, and assessed whether HS131 could label breast cancers with different molecular subtypes. As representative cell lines for each molecular subtype, MCF-7 and T-47D for luminal type, BT474M1 and KPL-4 for $HER2^+$ subtype, MDA-MB-231 and MDA-MB-468 for triple-negative subtype were chosen after considering the tumorigenic capacities of breast cancer cell lines in SCID mice. Cell surface Hsp90 expression of these breast cancer cell lines was analyzed *in vitro* by flow cytometry and shown in Supplementary Fig. S4.

Breast cancer cells were resuspended in 50% Matrigel/50% saline (1×10^6 cells/100 μL), and implanted subcutaneously to the flank of female SCID-beige mice. For MCF-7, T-47D, and BT474M1 cells, estrogen pellets were implanted to the back of mice to assist the tumor growth in mice. In addition, patient-derived breast cancer xenografts (PDX; HCI-013 EI, HCI-019) were maintained in SCID mice and used as breast cancers proximate to clinical cases. When the tumor sizes reached around 10 mm in diameter, HS131 or control HS152 were injected intravenously (10 nmol/mouse). Imaging was performed immediately after injection as well as at 3, 6, 12, and 24 hours after the administration of Hsp90 probes. As representative time points, images of immediate, 6-hour, and 24-hour time points are shown (Fig. 5). Importantly, all breast cancer xenografts with different molecular subtypes showed stronger nIR signals in tumor by intravenous administration of HS131 compared with HS152, and the retention of the nIR signals was detectable even at the 24-hour time point in HS131-injected mice.

To obtain the temporal dynamics of breast cancer imaging with HS131, we tested human triple-negative breast cancer line, MDA-MB-468. When the size of MDA-MB-468 tumors reached around 10 mm in diameter, HS131 or HS152 was administered to mice as described above. Whole-body images were acquired over time. As shown in Fig. 6A, control HS152 showed the peak level immediately after tail vein injection, and the nIR signal subsequently decreased by 3 hours after injection. However, HS131 showed strong nIR signals at the tumor area, and the peak level of nIR signals in the tumor area were almost 3 times higher than in HS152-injected mice. The nIR signals at the tumor area persisted for a longer duration in HS131-injected mice, such that 7 days after injection, nIR signals were still detectable (Fig. 6B), indicating prolonged intratumoral retention of HS131. Tumor-background ratio of nIR signal was calculated using nIR signal of the ear as a background, and shown for each compound (Fig. 6C). Tumor-to-background ratio reached the highest at the 24-hour time point in HS131-injected mice, and then gradually declined, while HS152 showed no increase after the 6-hour time point. Thus, the efficient uptake and longer retention of HS131 in tumors was demonstrated.

To confirm the accumulation of HS131 in human breast cancer tissues, the mice were euthanized at 24 hours after intravenous injection of HS131 or HS152 (10 nmol/injection), and tumors were harvested for *ex vivo* imaging. Tumors from mice received no HS131 or HS152 injection were used as negative controls. As shown in Fig. 6D and E, MDA-MB-231 tumors from mice injected with HS131 had significantly stronger nIR signal than tumors from HS152-injected mice. At 4 weeks after subcutaneous injection of MDA-MB-231 tumors, we observed lung metastasis in

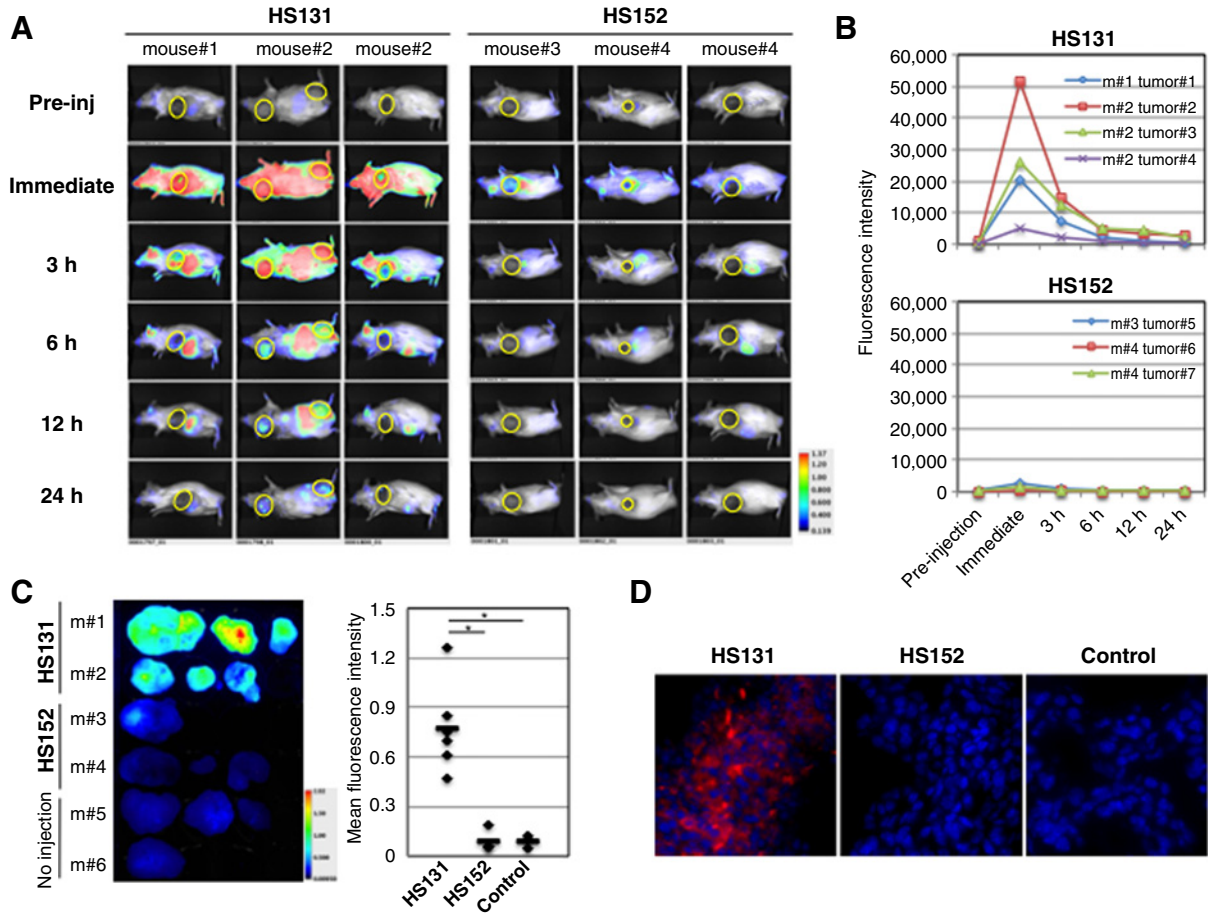

Figure 4.

In vivo imaging of spontaneous breast cancer with HS131. **A,** Temporal dynamics of nIR signal in MMTV-neu mice administered with HS131 or HS152. Female MMTV-neu mice were maintained for over 7 months, and mice with developing spontaneous breast cancers were used for imaging experiment with HS131 and HS152. Most of mice were around 8 to 10 months old, and tumor diameters varied from 5 mm to 15 mm. HS131 or HS152 (25 nmol/injection) were intravenously injected to mice via tail vein, and images were taken by LI-COR Pearl imager over time (immediate, 3, 6, 12, and 24 hours after HS131/HS152 injection). Mouse #1 and #3 had a single tumor, but mouse #2 and #4 had multiple tumors, and thus images were taken twice with different postures. Tumor areas are marked with yellow circles. **B,** Temporal dynamics of nIR signal from spontaneous breast tumors in *in vivo* imaging. Fluorescence intensities were monitored for individual tumors over time by LI-COR Pearl Imager, and plotted in the graphs. **C,** *Ex vivo* imaging of excised spontaneous breast tumors in MMTV-neu mice. Twenty-four hours after HS131/HS152 injection (25 nmol/injection) via tail vein, mice were euthanized and tumors were excised for *ex vivo* imaging. With 700-nm channel, nIR signals from tumors were detected *ex vivo*, and fluorescence intensities per area were calculated for individual tumors and plotted. Mouse number: HS131 ($n = 6$), HS152 ($n = 4$), no injection ($n = 4$). *, $P < 0.005$. **D,** Fluorescence microscope analysis of HS131 uptake in spontaneous breast tumor tissues. Excised tumor tissues were frozen using OCT compound. Sections were briefly fixed with 5% formalin, and DAPI containing mounting buffer was applied. Tissue were analyzed using Axio Observer Microscope with Cy5 cube (excitation: BP640/30, beam splitter: FT660, emission: BP690/50). DAPI: blue, nIR: red. Original magnification, 63× objective.

some mice (yellow arrows in Fig. 6D, right), and strong nIR signal was confirmed from these lung metastatic nodules. MDA-MB-231 tumors were excised from mice at the 6 hour and 24 hour time points after intravenous injection of HS131 or HS152, and digested with enzyme buffer as described in the Materials and Methods section. Cells obtained after tumor digestion were acquired by flow cytometry, and the nIR signal from tumor cells was analyzed by gating on larger cells with higher granularity in FSC/SSC (red line histogram). Gray histograms show tumor cells from mice without Hsp90 probe treatment. We confirmed that HS131-labeled MDA-MB-231 tumor cells *in vivo* at the 6- and 24-hour time points (Fig. 6F), while HS152 yielded no nIR signals from tumor cells.

Histologic analysis demonstrated diffuse nIR signals in the cytosol of HS131-exposed tumor cells as well as focal accumulation in vesicles. Control HS152 did not accumulate in the tumor cells to the same intense level, but only very weak nIR signal was observed (Fig. 6G). Thus, we confirmed the efficient *in vivo* labeling of human breast cancer cells by HS131.

Discussion

Breast cancer is a heterogeneous disease comprising different clinical, histopathologic, and molecular subtypes. Despite our understanding of the genetic and genomic aberration in breast cancer, we continue to detect and initially image breast cancer

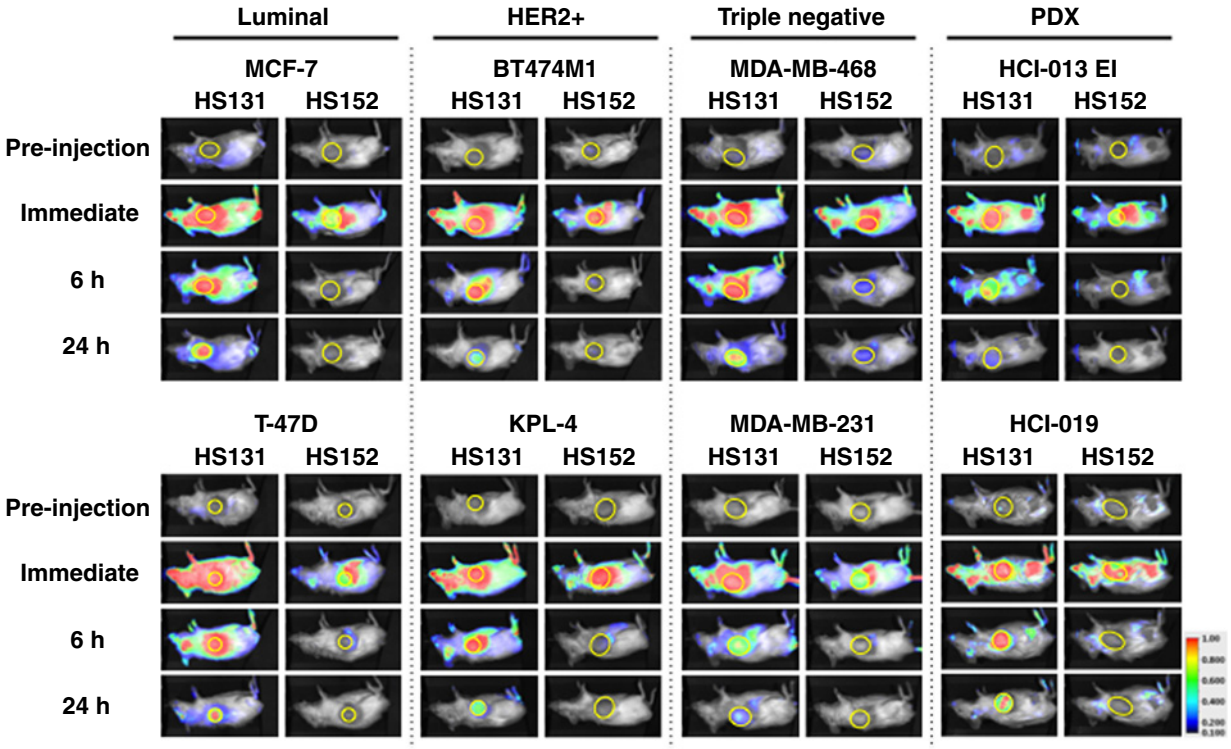

Figure 5.

In vivo imaging of human breast cancer xenografts of various molecular subtypes with HS131. Human breast cancer cell lines with various molecular subtypes (luminal, HER2^{+}, triple negative) were implanted subcutaneously to the flank of female SCID-beige mice (6–8 week old). For MCF-7, T-47D, and BT474M1 cells, estrogen pellets were implanted to the back of mice to enhance the tumor growth in mice. Patients' derived breast cancer xenografts (HCI-013 EI, HCI-019) were maintained in SCID mice by *in vivo* passage. When the tumor sizes reached around 10–12 mm in diameter, mice received administration of HS131 or control HS152 (10 nmol/mouse) via tail vein. nIR signals from these mice were analyzed over time (immediate, 3, 6, 12, 24, 72 hours, and 168 hours after compound injection) with LI-COR Pearl imager using 700-nm channel. Imaging was performed over time immediate, 3, 6, 12, and 24 hours after the administration of HS131 or HS152. As representative time points, images of immediate, 6, and 24-hour time points are shown. Tumor areas are marked with yellow circles.

based on a century old technology, specifically radiographic imaging to detect anatomic changes in the breast associated with growth and/or the radiographically detectable changes following necrotic events associated with growth. In contrast to these anatomic changes, more recently there has been a general definition of cancer focused on molecular changes, many of them manifested by aberrant signaling (1, 2), so called "hallmarks of cancer" (1). Consequently, we propose that the earliest diagnosis of breast cancer may occur when these "hallmarks of cancer" may be anatomically detected. Although detecting any one signaling aberration may be insufficient, an alternative may be to identify a global marker of aberrant signaling.

Candidates for a global marker of cancer signaling include the chaperone proteins such as Hsp90, which play critical roles for the expression and stability of hundreds of client proteins. Hsp90 has over 400 identified clients, many of which are oncogenic, and is known to be highly active in cancer (4–10). To identify high levels of cellular Hsp90, we exploited the known high affinity for Hsp90 of specific Hsp90 inhibitors to deliver an Hsp90 inhibitor–linked imaging compound (HS131) to cancers cells. It is well established that high levels of Hsp90 mRNA expression and protein levels are associated with clinically more aggressive breast cancers (8, 9). Therefore, we hypothesized that greater HS131 uptake would be associated with those tumors with more aggressive malignant behavior *in vivo*. Indeed, using variants of the murine TNBC 4T1 with a range of metastatic potentials (24), we observed greater levels of HS131 accumulation in the highly metastatic variants compared with the less metastatic variants (Figs. 2 and 3). Furthermore, we observed that the surface expression of Hsp90 (demonstrated using FACS analysis with Hsp90-specific antibodies in nonpermeabilized cells), correlated with metastatic potential (Fig. 2A). These data were confirmed for human breast cancer by demonstrating very high uptake of HS131 in the metastatic lesions of human tumor xenografts (Fig. 6). A similar correlation of Hsp90 surface expression with aggressive behavior was reported in malignant melanoma cases using flow cytometric and IHC analyses (25). This surface Hsp90 expression may represent one mechanism of HS131 uptake into malignant cells as demonstrated in our previous studies (16, 21). Another mechanism for increased HS131 levels in more aggressive tumors is their longer retention of HS131 (Fig. 6A–G).

To demonstrate the global ability of HS131 imaging to detect oncogenic signaling, we generated an isogenic model of murine breast tumors by transfecting a variety of oncogenes into MM3MG, a premalignant murine mammary cell line. In all of the oncogenes tested, resulting in typical malignant behaviors in

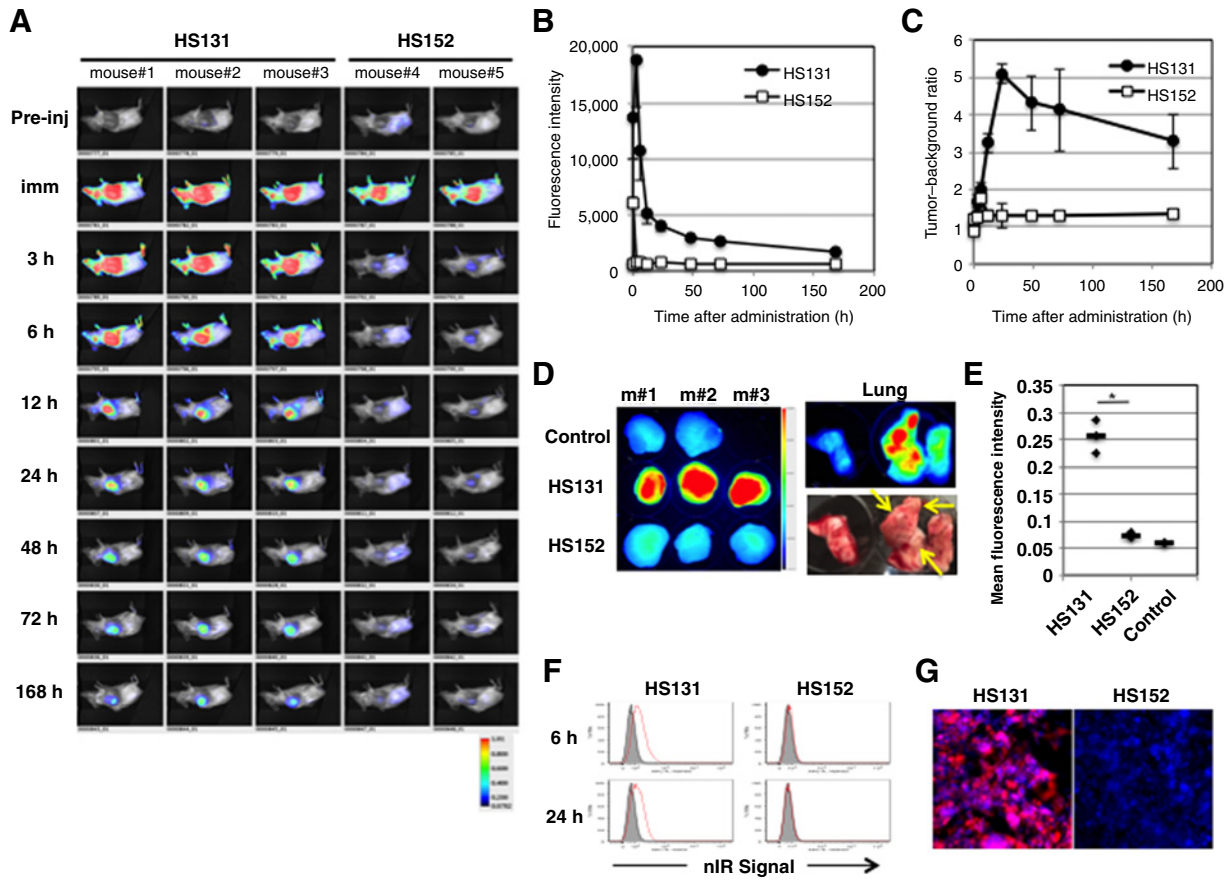

Figure 6.

In vivo imaging of human triple-negative breast cancer xenograft with HS131. **A,** nIR signal in MDA-MB-468 tumor-bearing SCID mice administered with HS131 or HS152. MDA-MB-468 tumor-bearing SCID-beige mice received administration of HS131 or control HS152 (10 nmol/mouse) via tail vein. nIR signals from these mice were analyzed over time (immediate, 3, 6, 12, 24, 72, and 168 hours after compound injection) with LI-COR Pearl Imager using 700-nm channel. Mouse 1, 2, and 3 were injected with HS131, while mouse 4 and 5 were inoculated with HS152. **B,** Temporal dynamics of nIR signal from MDA-MB-468 tumors. Average fluorescence intensities measured by the LI-COR Pearl imager for each treatment group (HS131, HS152) were calculated and plotted in the graph. Error bar, SD. **C,** Tumor-to-background ratio of nIR signal. Mean fluorescence intensities (MFI) of tumors and background areas (ear) were analyzed using Image Studio software. Tumor-to-background ratios were calculated by dividing MFI of tumors by MFI of background areas. Temporal dynamics of tumor-to-background ratios is shown. Filled circle: HS131, open square: HS152. Error bars, SD. **D,** *Ex vivo* imaging of MDA-MB-231 tumor xenografts. MDA-MB-231 tumor-bearing SCID-beige mice received administration of HS131 or control HS152 (10 nmol/mouse) via tail vein. Twenty-four hours after nIR-HSP90 inhibitor compound injection, mice were euthanized and flank tumors were excised. nIR signals from tumor were analyzed *ex vivo* with LI-COR Pearl imager by using 700-nm channel. Tumors from 3 mice for each compound were used for the imaging. MDA-MB-231 xenografts without nIR-HSP90 inhibitor injection to mice were used as negative controls for imaging. Right, metastatic lung nodules and nIR images of the same lung area in HS131-injected mouse are shown. Yellow arrows show metastatic nodules. **E,** MFI of MDA-MB-231 tumors by *ex vivo* imaging. Fluorescence intensities per area for each tumor are shown. *, $P < 0.001$. **F,** Flow cytometry analysis of HS131 uptake *in vivo* by MDA-MB-231 tumor cells. MDA-MB-231 tumor-bearing mice were administered with HS131 or HS152 (10 nmol/injection) via tail vein 6 or 24 hours before euthanizing mice. Tumors were excised from euthanized mice, and single cells were harvested by mincing, followed by enzymatic digestion of tumor tissue. Cells were acquired by LSRII flow cytometry machine. Tumor cells harvested from control MDA-MB-231 tumors (mice received no HS131 or HS152 injection) were used as control cells. nIR signals of tumor cells (red open histogram) was overlayed with control histogram (gray filled). **G,** Fluorescence microscope analysis of HS131 uptake in MDA-MB-231 tumor tissues. Excised tumor tissues were fixed with 5% formalin overnight. Tissue were analyzed using Axio Observer Microscope with Cy5 cube (excitation: BP640/30, beam splitter: FT660, emission: BP690/50). DAPI: blue, nIR: red. Original magnification: 40× objective.

in vitro and *in vivo* assays, HS131 was clearly taken up and retained, enabling specific imaging of the tumors formed by these cells (Figs. 2F and 3D).

While these tumor models are informative, we also wanted to determine whether we could detect malignant cells within the ducts of mouse breast tissue. Each of these regions are critical locations that may be hypoxic or poorly perfused, but we demonstrated excellent visualization with HS131 of tumor cells injected into the breast duct via intraductal injection of tumor cells (Supplementary Fig. S3). In contrast to antibody-based imaging, and imaging using other macromolecules or nanotechnologies, the use of a small-molecule probe ensures wide biodistribution of the probe based on tissue diffusion, rather than delivery by extravasation from blood vessels that is highly dependent on tumor perfusion.

Another model of breast tumor includes the spontaneous tumors formed in the glands of genetically engineered mice. HS131 imagining was sensitive and specific in detecting tumors

in the MMTV-rat neu models. We found excellent contrast in intact animals, and found high degrees of tumor uptake when we harvested and imaged tumors *ex vivo* (Fig. 4).

While HS131 could detect different oncogenic signaling, we wished to confirm its ability to detect the various human molecular subtypes. Molecular studies have identified five main intrinsic subtypes: luminal A, luminal B, HER2-enriched, normal-like, and basal-like breast cancers (26). At the molecular level, classification and characterization of the breast cancer at the gene, messenger RNA, protein, and phosphoprotein level are component of precision medicine, using state of the art strategies to quantity these changes in collection of breast cancer specimens, but also in individual patients in a timeframe sufficient to make treatment management decisions.

Using human xenografts, we were able to image multiple examples of luminal, $HER2^+$, and TNBC subtypes and have not found a breast cancer line that could not be imaged. Therefore, we turned to patient-derived xenograft. We chose a PDX that represented an ER^+ luminal invasive lobular carcinoma. This is an important histologic subtype, as these represent about 10% of breast cancers, but are poorly imaged by mammography or breast MRI and often detected by palpation, presenting later stages (27–29). HS131 was highly effective in imaging invasive lobular carcinoma (Fig. 5).

In summary, nIR dye–tethered Hsp90 inhibitor (HS131) was able to detect oncogene-driven breast cancers, including multiple different molecular subtypes of human breast cancer, and stronger uptake was observed in cancers with higher metastatic potential. This supports initiation of clinical trials to detect early aggressive breast cancers and their metastases using Hsp90-targeting nIR probes. In addition to detecting and visualizing malignant tissue that will require management, this technology has a long-term potential for therapeutic intervention. For instance, conjugating a moiety that can be activated by laser light energy that can penetrate breast tissue may create a diagnostic and therapeutic modality that can sequentially detect and then ablate the malignant cells. Further work on developing appropriate cytotoxic agents conjugated to HSP90 probes may also improve systemic delivery to metastatic lesions.

Disclosure of Potential Conflicts of Interest

T. Haystead and P.F. Hughes are coinventors on a US patent (9738643B2) "Substituted indazoles for targeting Hsp90" which is owned by Duke University and is currently unlicensed. No potential conflicts of interest were disclosed the other authors.

Authors' Contributions

Conception and design: T. Osada, M.A. Morse, A. Hobeika, P.F. Hughes, T. Haystead, H.K. Lyerly

Development of methodology: T. Osada, P.F. Hughes, T. Haystead, H.K. Lyerly

Acquisition of data (provided animals, acquired and managed patients, provided facilities, etc.): T. Osada, K. Kaneko, Z.C. Hartman, H.K. Lyerly

Analysis and interpretation of data (e.g., statistical analysis, biostatistics, computational analysis): T. Osada, K. Kaneko, W.R. Gwin, M.A. Morse, B.W. Pogue, T. Haystead, H.K. Lyerly

Writing, review, and/or revision of the manuscript: T. Osada, W.R. Gwin, M.A. Morse, B.W. Pogue, P.F. Hughes, T. Haystead, H.K. Lyerly

Administrative, technical, or material support (i.e., reporting or organizing data, constructing databases): M.A. Morse, A. Hobeika, Z.C. Hartman, P.F. Hughes, H.K. Lyerly

Study supervision: M.A. Morse, T. Haystead, H.K. Lyerly

Other (designed and made the organic compounds used in this article): P.F. Hughes

Acknowledgments

This work was supported by a grant from the Department of Defense (TVA W81XWH-12-1-0447; grant no. BC111085).

The authors thank Drs. Xiao Yang, Cong-Xiao Liu, and Tao Wang for the technical assistance.

The costs of publication of this article were defrayed in part by the payment of page charges. This article must therefore be hereby marked *advertisement* in accordance with 18 U.S.C. Section 1734 solely to indicate this fact.

Received May 19, 2017; revised July 29, 2017; accepted October 3, 2017; published OnlineFirst October 9, 2017.

References

1. Hanahan D, Weinberg RA. Hallmarks of cancer: the next generation. Cell 2011;144:646–74.
2. Srivastava S, Grizzle WE. Biomarkers and the genetics of early neoplastic lesions. Cancer Biomark 2010;9:41–64.
3. Echeverría PC, Forafonov F, Pandey DP, Mühlebach G, Picard D. Detection of changes in gene regulatory patterns, elicited by perturbations of the Hsp90 molecular chaperone complex, by visualizing multiple experiments with an animation. BioData Min 2011;4:15.
4. Moulick K, Ahn JH, Zong H, Rodina A, Cerchietti L, Gomes DaGama EM, et al. Affinity-based proteomics reveal cancer-specific networks coordinated by Hsp90. Nat Chem Biol 2011;7:818–26.
5. Neckers L, Mollapour M, Tsutsumi S. The complex dance of the molecular chaperone Hsp90. Trends Biochem Sci 2009;34:223–6.
6. Samant RS, Clarke PA, Workman P. The expanding proteome of the molecular chaperone HSP90. Cell Cycle 2012;11:1301–8.
7. Vaughan CK, Neckers L, Piper PW. Understanding of the Hsp90 molecular chaperone reaches new heights. Nat Struct Mol Biol 2010;17:1400–4.
8. Pick E, Kluger Y, Giltnane JM, Moeder C, Camp RL, Rimm DL, et al. High HSP90 expression is associated with decreased survival in breast cancer. Cancer Res 2007;67:2932–7.
9. Cheng Q, Chang JT, Geradts J, Neckers LM, Haystead T, Spector NL, et al. Amplification and high-level expression of heat shock protein 90 marks aggressive phenotypes of human epidermal growth factor receptor 2 negative breast cancer. Breast Cancer Res 2012;14:R62.
10. Whitesell L, Lindquist SL. HSP90 and the chaperoning of cancer. Nat Rev Cancer 2005;5:761–72.
11. Tsutsumi S, Neckers L. Extracellular heat shock protein 90: a role for a molecular chaperone in cell motility and cancer metastasis. Cancer Sci 2007;98:1536–9.
12. Tsutsumi S, Scroggins B, Koga F, Lee MJ, Trepel J, Felts S, et al. A small molecule cell-impermeant Hsp90 antagonist inhibits tumor cell motility and invasion. Oncogene 2008;27:2478–87.
13. Eustace BK, Sakurai T, Stewart JK, Yimlamai D, Unger C, Zehetmeier C, et al. Functional proteomic screens reveal an essential extracellular role for hsp90 alpha in cancer cell invasiveness. Nat Cell Biol 2004;6: 507–14.
14. McCready J, Sims JD, Chan D, Jay DG. Secretion of extracellular hsp90alpha via exosomes increases cancer cell motility: a role for plasminogen activation. BMC Cancer 2010;10:294.
15. Sims JD, McCready J, Jay DG. Extracellular heat shock protein (Hsp)70 and Hsp90α assist in matrix metalloproteinase-2 activation and breast cancer cell migration and invasion. PLoS One 2011;6:e18848.
16. Crowe LB, Hughes PF, Alcorta DA, Osada T, Smith AP, Totzke J, et al. A fluorescent Hsp90 probe demonstrates the unique association between extracellular Hsp90 and malignancy *invivo*. ACS Chem Biol 2017;12: 1047–55.
17. Tsutsumi S, Beebe K, Neckers L. Impact of heat-shock protein 90 on cancer metastasis. Future Oncol 2009;5:679–88.

18. Chiosis G, Lucas B, Huezo H, Solit D, Basso A, Rosen N. Development of purine-scaffold small molecule inhibitors of Hsp90. Curr Cancer Drug Targets 2003;3:371–6.
19. Csermely P, Schnaider T, Soti C, Prohászka Z, Nardai G. The 90-kDa molecular chaperone family: structure, function, and clinical applications. A comprehensive review. Pharmacol Ther 1998;79:129–68.
20. Fadden P, Huang KH, Veal JM, Steed PM, Barabasz AF, Foley B, et al. Application of chemoproteomics to drug discovery: identification of a clinical candidate targeting hsp90. Chem Biol 2010;17:686–94.
21. Barrott JJ, Hughes PF, Osada T, Yang XY, Hartman ZC, Loiselle DR, et al. Optical and radioiodinated tethered Hsp90 inhibitors reveal selective internalization of ectopic Hsp90 in malignant breast tumor cells. Chem Biol 2013;20:1187–97.
22. Lee C, Dhillon J, Wang MY, Gao Y, Hu K, Park E, et al. Targeting YB-1 in HER-2 overexpressing breast cancer cells induces apoptosis via the mTOR/STAT3 pathway and suppresses tumor growth in mice. Cancer Res 2008;68:8661–6.
23. Kurebayashi J, Otsuki T, Tang CK, Kurosumi M, Yamamoto S, Tanaka K, et al. Isolation and characterization of a new human breast cancer cell line, KPL-4, expressing the Erb B family receptors and interleukin-6. Br J Cancer 1999;79:707–17.
24. Aslakson CJ, Miller FR: Selective events in the metastatic process defined by analysis of the sequential dissemination of subpopulations of a mouse mammary tumor. Cancer Res 1992, 52:1399–405.
25. Becker B, Multhoff G, Farkas B, Wild PJ, Landthaler M, Stolz W, et al. Induction of HSP90 protein expression in malignant melanomas and melanoma metastases. Exp Dermatol 2004;13:27–32.
26. Perou CM, Sorlie T, Eisen MB, van de Rijn M, Jeffrey SS, Rees CA, et al. Molecular portraits of human breast tumours. Nature 2000;406:747–52.
27. Helvie MA, Paramagul C, Oberman HA, Adler DD. Invasive lobular carcinoma. Imaging features and clinical detection. Invest Radiol 1993; 28:202–7.
28. Molland JG, Donnellan M, Janu NC, Carmalt HL, Kennedy CW, Gillett DJ. Infiltrating lobular carcinoma – a comparison of diagnosis, management and outcome with infiltrating duct carcinoma. Breast 2004;13:389–96.
29. Cornford EJ, Wilson AR, Athanassiou E, Galea M, Ellis IO, Elston CW, et al. Mammographic features of invasive lobular and invasive ductal carcinoma of the breast: a comparative analysis. Br J Radiol 1995;68:450–3.

Clinical Cancer Research

In Vivo Detection of HSP90 Identifies Breast Cancers with Aggressive Behavior

Takuya Osada, Kensuke Kaneko, William R. Gwin, et al.

Clin Cancer Res 2017;23:7531-7542. Published OnlineFirst October 9, 2017.